Frontiers in Health Informatics
ISSN-Online: 2676-7104
www.healthinformaticsjournal.com
2024; Vol 13: Issue 4
Open Access

Fabrication of High-Performance (Cu, N)-CodopedTiO$_2$ Photocatalyst for solar Light-Induced Mineralization of Metanil Yellow

S. Cathaline Jagha
Research Scholar, (Reg.No.20123112032016), Department of Chemistry and Research, Nesamony Memorial Christian College, Marthandam (Affiliated to Manonmaniam Sundaranar University, Abishekapatti, Tirunelveli), Tamilnadu, India.

Dr. E. K. Kirupa Vasam
Assistant Professor, Department of Chemistry and Research, Nesamony Memorial Christian College, Marthandam, (Affiliated to Manonmaniam Sundaranar University, Abishekapatti, Tirunelveli), Tamilnadu, India.

Cite this paper as: S. Cathaline Jagha, Dr. E. K. Kirupa Vasam (2024) Fabrication of High-Performance (Cu, N)-CodopedTiO2 Photocatalyst for solar Light-Induced Mineralization of Metanil Yellow. *Frontiers in Health Informatics,* (4), 2152-2182

Abstract

In this study, visible-light-active (Cu, N)-codoped TiO_2 photocatalyst were synthesized via a sol–gel method using titanium tetraisopropoxide (TTIP) as the precursor. The structural, optical, morphological, and elemental characteristics of the synthesized photocatalysts were comprehensively analyzed using XRD, FT-IR, SEM-EDX, HR-TEM, and UV–Vis DRS techniques. MetanilYellow (MY), an azo dye, was selected as a model pollutant to evaluate the photocatalytic efficiency of the synthesized (Cu, N)-codopedTiO$_2$ photocatalyst under visible-light irradiation. The results revealed that the (Cu, N)-codopedTiO$_2$ photocatalyst (0.15g/100mL) completely degraded MY (20ppm) within 40 minutes under visible-light exposure. Furthermore, Chemical Oxygen Demand (COD) and Total Organic Carbon (TOC) analysis confirmed a 99% mineralization rate. The degradation reaction followed pseudo-first-order kinetics with an apparent rate constant of $\mathbf{0.051}\times10^{-3}$ $\mathbf{min^{-1}}$ (R^2 = 0.978). The photocatalyst exhibited excellent stability and reusability, maintaining high efficiency for up to five consecutive cycles without significant loss of activity. The enhanced photocatalytic performance of the (Cu, N)-codopedTiO$_2$ is attributed to the effective suppression of electron–hole recombination. The synthesized nanoparticles were stable, well-crystallized, and environmentally benign, making them suitable for the treatment of organic pollutants in industrial and agricultural wastewater under sunlight. Therefore, the fabricated (Cu, N)-codopedTiO$_2$ photocatalyst was found to be an efficient and cost-effective material as only a small amount of photocatalyst is required for environmental remediation applications.

Keywords:*CodopedTiO$_2$ Photocatalyst**, Visible Light, Metanil Yellow, Pollutant, photodegradation,,Mineralisation*

Abbreviations			***Nomenclatures***	
AOPs	Advanced Oxidation Processes		Al_2O_3	Aluminum oxide (or) Alumina

COD	Chemical Oxygen Demand		V_2O_5	Vanadium pentoxide
DRS	Diffuse Reflectance Spectroscopic		WO_3	Tungsten trioxide
EDX	Energy Dispersive X-Ray		CO_2	Carbon dioxide
FT-IR	Fourier Transform Infrared		H_2O	Water
HR-TEM	High-Resolution Transmission Electron Microscope		O_2	Oxygen
IR	Infrared		$O_2^{\bullet-}$	Superoxide radical anions
JCPDS	Joint Committee on Powder Diffraction Standards		ZnO	Zinc Oxide
MY	Metanil Yellow		N	Nitrogen
SEM	Scanning Electron Microscope		OH	Hydroxyl
TOC	Total Organic Carbon		ZrO_2	Zirconium dioxide
TTIP	Titanium Tetraisopropoxide		Cu	Copper
UV	Ultraviolet		CuO	Cupric oxide
XRD	X-Ray Diffraction		TiO_2	Titanium dioxide (or) Titania
			SnO_2	Stannic oxide
			NiO	Nickel monoxide

INTRODUCTION

One of the key challenges in managing water utility in industries is the disposal of wastewater. The discharge of industrial wastewater can lead to severe environmental and health consequences [1]. Wastewater containing dyes is a significant environmental pollutant and poses serious risks to human health, as textiles generate large amounts of highly colored wastewater containing a diverse range of persistent pollutants [2]. Textile wastewater has been found to contain a wide range of toxic dyes and heavy metals, such as mercury, chromium, cadmium, lead, and arsenic, which are used in the production of textile dye color pigments, as well as aromatic compounds [3]. These toxic chemicals are transported over long distances together with wastewater and remain in the water and soil for long periods, posing serious health risks to living organisms, reducing soil fertility, and affecting the photosynthetic activity of aquatic plants, which can result in anoxic conditions for aquatic fauna and flora [4].

Hence, it is vital to remove such dyes from industrial wastewater before it is discharged into natural water bodies [5]. Conventional water treatment technologies, such as adsorption, coagulation, sedimentation, filtration, and chemical and membrane-based approaches, are often insufficient for complete dye degradation [6, 7]. Therefore, advanced oxidation processes (AOPs) are employed to remove soluble dyes. Among these, photocatalysis is a promising technique that uses light and catalysts to accelerate the degradation of organic pollutants [8]. Previous studies indicate that photocatalysis can remove 70–80% of pigments from industrial effluents.

Semiconductor nanomaterials absorb energy greater than their bandgap, which excites electrons from the valence band to the conduction band, generating electron–hole pairs. When a metal oxide nanoparticle is exposed to UV–Vis radiation, electrons are excited to the conduction band and electron-

hole pairs are created [9]. The valence band holes react with surface-bound H_2O to produce hydroxyl (•OH) radicals, while the electrons react with oxygen (O_2) molecules to produce superoxide radical anions ($O_2^{\bullet-}$) [10]. These reactive species oxidize organic dyes, degrading them into carbon dioxide(CO_2), water (H_2O), and other mineralized products [11].

MY isselected as a model test pollutant for the present study due to itstoxic nature and extensive application in several industrial sectors like textile, leather, shoe polish, wood stain, paper, food, and cosmetics [12]. Exposure to this dye can cause tumors, anemia, intestinal disorders, and contact dermatitis upon direct skin contact [13]. Therefore,it is necessary to treat industrial effluents before discharging into nearby freshwater streams [14].Many conventional treatment methods are used for treating industrial effluents including physical, chemical and biological processes. However these methods have several limitations. In contrast, semiconductor-mediated photocatalytic mineralisation of effluent serves as a promising technology, as complete mineralisation is possible at room temperature in the presence of very small amount of photocatalyst(Chong et al. 2010).

ZnO [15], TiO_2 [16], CuO [17], WO_3 [18], V_2O_5 [19], ZrO_2 [20], Al_2O_3 [21], SnO_2 [22], and NiO [23] are among the metal oxide-based semiconductors recently used in photocatalysis. Among these, TiO_2 is preferred due to its non-toxic nature,and excellent properties such as low resistivity, high thermal and chemical stability, high optical transmittance, and strong photocatalytic activity [24]. However, the photocatalytic efficiency of TiO_2 is limited due to its wide bandgap (3.3eV), its UV-light-dependent excitation, and the highrecombination rate of electron-hole pairs (e^-/h^+)[25]. To overcome these limitations, co-doping of $TiO_2$with metals and/or non-metals has been explored to enhance its solar-light absorption andreduce electron-hole recombination.

According to literature reported, non-metaldoping narrows the bandgap of TiO_2,allowing it to absorb visible light instead of being restricted to the UV region which significantly improve its photocatalytic activity (Asahi et al. 2014). Shahid [26] reported that 1% Cu/Zr co-doped TiO_2 (CZTO) nanoparticles achieved 92% degradation of methylene blue within 120 minutes under visible light, with an apparent rate constant 4.6 times higher than that of pure TiO_2. Getye B Y et al. demonstrated that a TiO_2/CuO nanocomposite photocatalyst achieved 99% degradation of methylene blue within 90 minutes under visible light, following pseudo-first-order kinetics with good stability and reusability [27]. Sirivallopet al. showed that 5% N and Ag co-doped TiO_2 achieved 98.82% degradation of methylene blue under visible light in 6 hours, with a significant enhancement due to synergisticeffect of N and Ag doping [28]. Faustino E et al. reported that N- and Fe-codopedTiO_2 nanoparticles achieved 92% mineralization of 2,4-dimethylaniline under UV light within 180 minutes; optimal doping of Fe(0.0125% Fe)on TiO_2 has reduced the bandgap to 2.82 eV and thus increased the surface area to 84.73 m^2/g, due to the synergistic effect of N and Fe doping [29].N-doped and Cu-doped TiO_2 have been reported for the photodegradation of various dyes,whereas limited research is available on Cu and N co-doped TiO_2 on dye degradation**,** highlighting the novelty and significance of the present study.

This study focuses on synthesizing undoped TiO_2 and (Cu,N)co-doped TiO_2 photocatalyst via sol-gel method to improve photocatalytic activity. Metal ions such as Cu^{2+}, Ni^{2+}, Co^{3+}, and Fe^{3+} act as

charge carriers, while nitrogen doping introduces 2p states above the valence band, narrowing the bandgap for visible-light absorption. Cu serves as an electron trap, and N improves hole mobility, reducing electron-hole recombination. Co-doping also generates oxygen vacancies and enhances surface reactivity, resulting in superior photocatalytic activity compared to undoped TiO_2 [30].

The synthesized (Cu,N)-codopedTiO_2 photocatalyst was characterized using UV–DRS, TEM, SEM, XRD, and FT-IR analysis, confirming the successful incorporation of dopants into the TiO_2 lattice. Photocatalytic efficiency was evaluated via the degradation of MY under sunlight, and mineralization was confirmedthrough COD and TOC analysis. Furthermore, the quality and durability of the (Cu, N)-codopedTiO_2 photocatalyst were confirmed by recycling it over five successive cycles, demonstrating its stability and reusability for environmental remediation applications.

EXPERIMENTAL METHODS

Materials

The chemicals required for the present study includes: Titanium tetraisopropoxide, (TTIP)$Ti[OCH(CH_3)_2]_4$,Urea (NH_2CONH_2), Copper (II) nitrate trihydrate ($Cu(NO_3)_2.3H_2O$), and absolute ethanol (C_2H_6O) (99%) purchased from Merck Specialties Pvt Ltd., Mumbai and ISO-Chem Laboratories, Kochi respectively. These chemicals were procured for the fabrication of (Cu, N)-codopedTiO_2 photocatalyst and are used in pristine form. Double-distilled water is used for all the experimental studies. The photocatalytic irradiation were carried out from 11:00 AM to 2:00 PM on sunny days. For this investigation, Metanil yellow ($C_{18}H_{14}N_3NaO_3S$) was chosen as the test pollutant. Table 1 shows the physicochemical properties of Metanilyellowdye.

Table1. Physicochemical properties of MY

Table1. Physicochemical properties of MY dye

Property	Description
UPAC name	I sodium 3-[(E)-(4-anilinophenyl)diazenyl]benzenesulfonate
Molecular formula	$C_{18}H_{14}N_3NaO_3S$
Structure	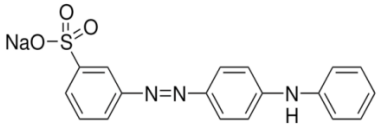
Molecular weight	375.38 g/mol
Physical state	Solid and powder
Melting point	greater than 250°C
Water solubility	soluble in Water
Number of azo bonds	one
Maximum absorption wavelength	439 nm

Synthesis of undoped TiO_2 and (Cu,N)-codopedTiO_2photocatalysts

Synthesis of undoped TiO_2

To synthesize undoped TiO_2, 10 mL of titanium isopropoxide (TTIP) was mixed with 40 mL of ethanol under constant stirring.5 mL of deionized water was mixed with 20 mL of ethanol in a separate container, andfew drops ofnitric acid is added to control the pH. The ethanol-water mixturewas added dropwise into the TTIP solution undercontinuousstirring to form a white gel.The gel is allowed to stand at room temperaturefor agingto about 24 hours. After aging, the gels dried in an hot air oven at 80-100°C to remove the solvents. Finally, the dried material isheated in a muffle furnace at around 450–500°C for 2–4 hours to obtain crystalline TiO_2 in the anatase phase. Fig 1a represents the undoped TiO_2 synthesised by the above method

Synthesis of (Cu,N)-codopedTiO_2 photocatalyst

Fig 1b represents the synthesized (Cu,N)-codopedTiO_2 photocatalyst for the present mineralistion of metanil yellow dye.

8.9 mL of Titanium (IV) isopropoxide (TTIP) was dissolved in 140 mL of absolute alcohol and continuously stirred for 15 min. About 2 mL of distilled water was added.The suspension was stirred for 45 min and 1 M HCl was added to adjust the pH to 3. To this solution, desired amount of urea and copper (II) nitrate trhydrate was added, and the solution was allowed for aging for about 24 hours to form a gel. The collected gel was dried at 105°C for about 24 hours, and calcined at500°C to about 2 h in a muffle furnace, to form Cu–N co-doped TiO_2 photocatalyst[31].

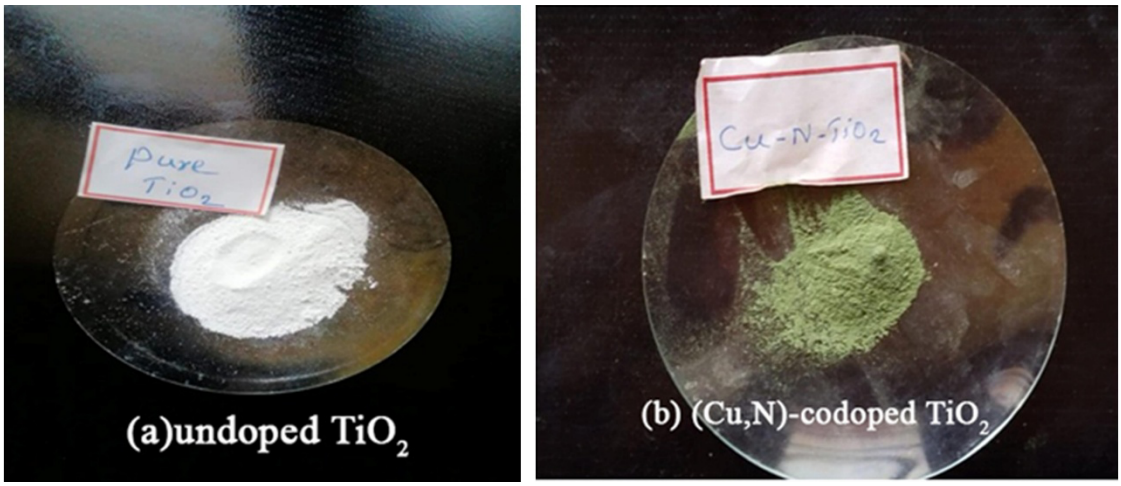

Fig. 1. Synthesized samples of (a) undoped TiO_2 and (b) (Cu,N)-codoped TiO_2 photocatalysts

Characterization techniques

Structural and crystalline phases of the synthesized nanophotocatalyst were characterized using an X-ray diffractometer (XRD, Bruker D8 Advance diffractometer) with Cu Kα radiation (λ = 0.154 nm), operated at 40 kV and 100 mA over a diffraction range (2θ) of 20°–80°. The structural analysis was performed using an FT-IR spectrometer (Thermo Nicolet 380) in the range of 400–4000 cm^{-1}. The surface morphology and elemental composition were examined using a scanning electron microscope

(SEM, JEOL 5800LV) and energy-dispersive X-ray spectrometry (EDS, JSM-100F), respectively. The transmission electron microscopy (TEM) images of the nanophotocatalyst were analyzed using a high-resolution transmission electron microscope (HR-TEM, JEOL 2100). Moreover, the UV-Vis diffuse reflectance absorption spectra (UV-Vis/DRS) were recorded in the range of 190–1100 nm using a Thermo Fisher Evolution 220 spectrophotometer equipped with an integrating sphere ($BaSO_4$ as the reference, 99% reflectance).

Photocatalytic degradation experiment

The photocatalytic degradation experiment was carried out using a photocatalytic reactor, as shown in Fig. 2. The stock solution for degradation studies was prepared by dissolving a known amount of MY dye in 100 mL of double-distilled water. A measured quantity of the synthesized undoped TiO_2 was added to the dye solution and its photocatalytic activity was analyzed. Parallel experiments were also conducted using the (Cu, N)-codopedTiO_2 photocatalyst.Initially, the dye–photocatalyst suspension was magnetically stirred in the dark for approximately 30 minutes to establish adsorption–desorption equilibrium. The suspension was then exposed to direct sunlight under continuous stirring. The photocatalytic performance of (Cu, N)-codopedTiO_2 was evaluated at regular intervals usingUV–Vis spectrophotometer by measuring the absorbance at λ_{max} = 427 nm corresponding to the maximum absorbance of MYdye under study.

The degradation efficiency was calculated using Equation (1).

$$degradation\ (\%) = {(C_0 - C_t)}\Big/{C_0 \times 100} \quad (1)$$

Here, C_0 refers to the initial concentration of the dye solution with adsorption–desorption equilibrium andC_t denotes the concentration of the dye solution after photocatalytic degradation under sunlight. Fig 2 represents the photocatalytic setup for the experimental study.

Fig. 2. Photocatalytic experimental setup

RESULTS AND DISCUSSION

XRD Analysis

The phase structure, composition, and average crystallite size of the synthesized undoped TiO_2 and (Cu, N)-codopedTiO_2 photocatalysts were analyzed using XRD, as shown in Fig. 3.

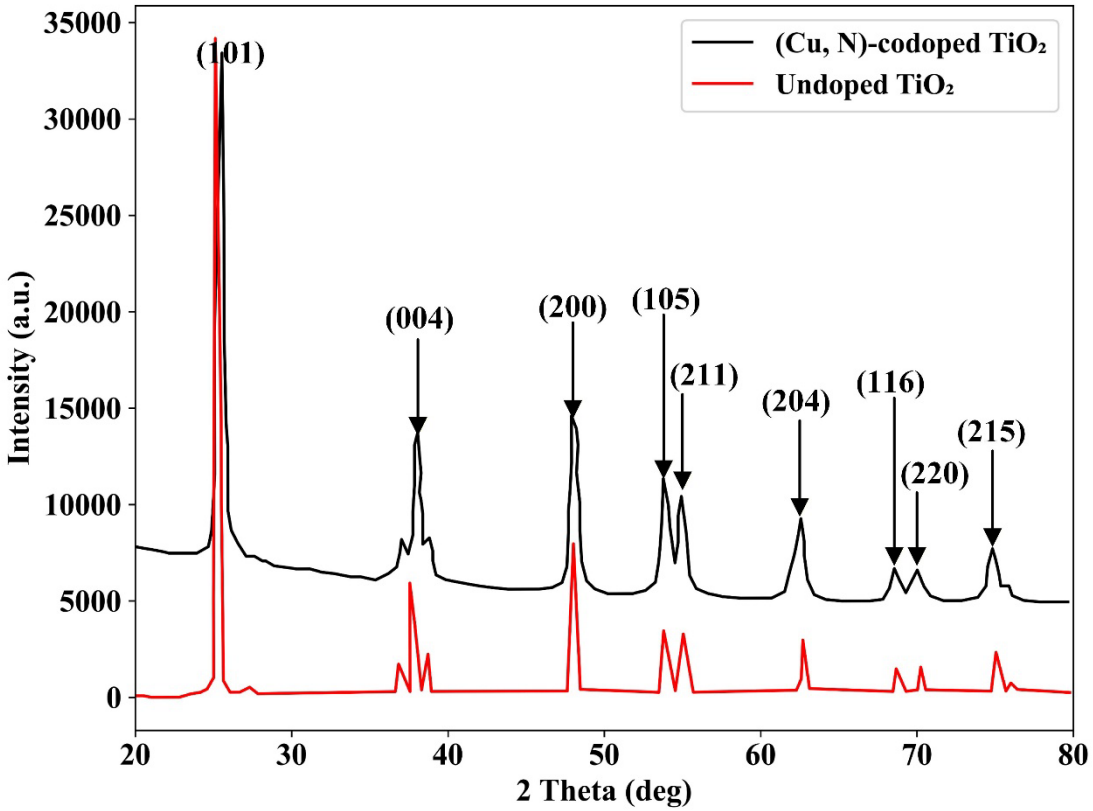

Fig.3. X-ray diffraction (XRD) patterns of undoped TiO_2 and (Cu,N)-codopedTiO_2

The XRD pattern of undoped TiO_2 exhibited peaks at 25.29°, 38.57°, 48.04°, 53.89°, 55.07°, 63.04°, 69.01°, 70.4°, and 75.2° corresponding to the anatase crystal planes (101), (121), (004), (200), (105), (211), (204), (116), (220), and (215) crystalline planes of anatase TiO_2 [32]. Similarly, the XRD pattern of synthesized (Cu, N)-codopedTiO_2 exhibited diffraction peaks at 25.30°, 39.01°, 44.24°, 48.04°, 53.92°, 55.92°, 55.09°, 58.06°, and 63.06°, corresponding to the crystal planes of (101), (121), (004), (200), (105), (211), (204), (116), (220), and (215) planes of the anatase phase, respectively. Among these, the (101) peak at 25.30° is the strongest, indicating that this plane has the dominant crystallographic orientation in the TiO_2 lattice. Moreover, these diffraction patterns agreed with (JCPDS) Card No. 21-1272.These results indicate that the anatase crystal structure of TiO_2 is preserved after co-doping with Cu and N. Slight shifts or broadening of peaks may occur due to lattice distortions caused by the incorporation of dopants, but no additional peaks corresponding to CuO or Cu_2O are observed, confirming the absence of separate copper oxide phases [33].

Electronegativity values of Ti^{4+} and Cu^{2+} are 1.5 and 1.9 respectively. Moreover, the ionic radius of Ti^{4+} is 0.745 Å, and Cu^{2+} is 0.870 Å [34]. The ionic radius of Cu^{2+} is higher than that of Ti^{4+} ions. Hence, Cu^{2+} ions are located in the interstitial positions in the lattice site of TiO_2 rather than directly in Ti^{4+} sites due to the relatively large size of the Cu^{2+} ions [35, 36]. The crystalline size of the synthesized

(Cu,N)-codopedTiO_2 photocatalyst was estimated by using the Debye-Scherrer formula as given in Equation (2) [37].

$$D = \frac{K\lambda}{\beta \cos\theta} \quad (2)$$

Where,D is the average crystalline size, K is a constant equal to 0.90, λ is the wavelength in angstroms (Å), β represents the full width at half maximum in radians and θ represents the diffraction angle in degrees.

Using the above Equation (2), the average crystal sizes of undoped TiO_2 and (Cu, N)-codopedTiO_2 nanoparticles were calculated to be 22 nm and 11.2 nm, respectively. This small size is advantageous because it provides a high surface-to-volume ratio, enhancing the material's reactivity and adsorption properties. The sharp and well-defined peaks indicate that the TiO_2 particles are highly crystalline. The absence of extra peaks also confirms that no impurity or secondary phases (like rutile or brookite) are present. Such crystallinity is essential for reproducible photocatalytic activity and structural stability during reactions [38].

FT-IR Analysis

FT-IR spectra of the synthesized undoped TiO_2 and (Cu,N)-codoped TiO_2 photocatalysts is shown in Fig. 4. The absorption peak observed around 3400 cm^{-1} in undoped TiO_2 is attributed to the stretching vibrations of surface hydroxyl groups and adsorbed water molecules. Specifically, thecharacteristic bands at 3485 cm^{-1} and 3500 cm^{-1} confirms the presence of -OH groups within the sample structure, arising from surface-adsorbed water and hydroxylating agents [39]. Thepeak at ~1631 cm^{-1} inCu and N co-doped TiO_2 corresponds to O–H bending of adsorbed water. It confirms surface hydroxyl groups, which act as active sitescrucial for enhancing photocatalytic activityof TiO_2 [40, 41].

The FT-IR bands around 1480 cm^{-1} and 1255 cm^{-1} in TiO_2 are indicative of specific vibrational modes within the material. The band near 1480 cm^{-1} is commonly associated with the bending and stretching vibrations of O-Ti-O linkages within the TiO_2 lattice structure [42]. The peak around 1255 cm^{-1} is generally related to the lattice vibrations. A clear absorption band observed at 400–800 cm^{-1} region corresponds to the characteristic Ti–O–Ti stretching vibrations of the TiO_2 lattice. Upon Cu–N co-doping, additional bands appeared at approximately 1470 cm^{-1} and 1250 cm^{-1}, which are attributed to Ti–N vibrations, while a new band below 1000 cm^{-1} corresponds to Cu–O vibrations. These spectral features confirm the successful incorporation of both Cu and N ions into the TiO_2 structure [43, 44].

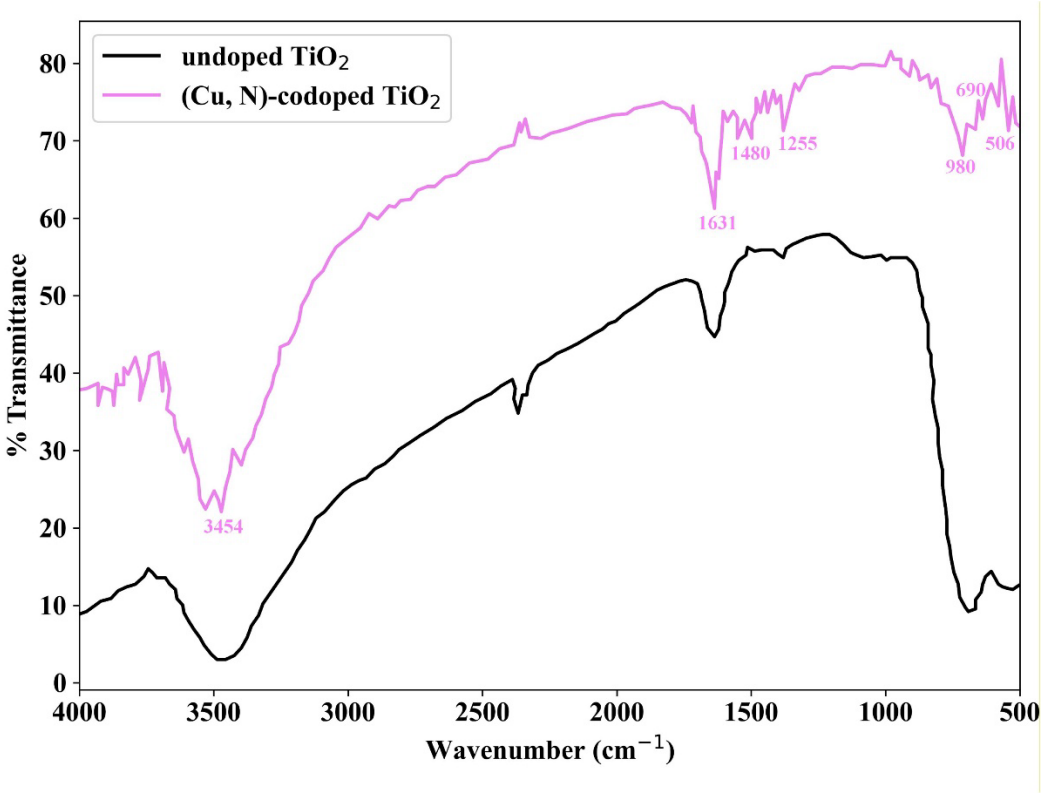

Fig.4. FT-IR Spectra for undoped TiO_2 and (Cu, N)-codoped TiO_2 photocatalysts.

SEM Analysis

The morphological and structural dimensions of undoped TiO_2 and (Cu, N)-codopedTiO_2 photocatalysts were investigated using scanning electron microscopy (SEM), as shown in Fig. 5(a) and Fig. 5(b), respectively. The SEM images revealthe undoped and (Cu, N)-codopedTiO_2 photocatalysts consist of nearly uniform nanoparticles exhibiting noticeable agglomeration. In the (Cu, N)-codopedTiO_2 sample (Fig. 5(b)), Cu and N atoms are uniformly distributed on the TiO_2 surface, indicating homogeneous doping without significant phase separation. Such agglomeration behavior is commonly observed in metal oxide nanoparticles and is primarily driven by the minimization of surface free energy during nanoparticlesynthesis and dryingprocesses [45, 46].

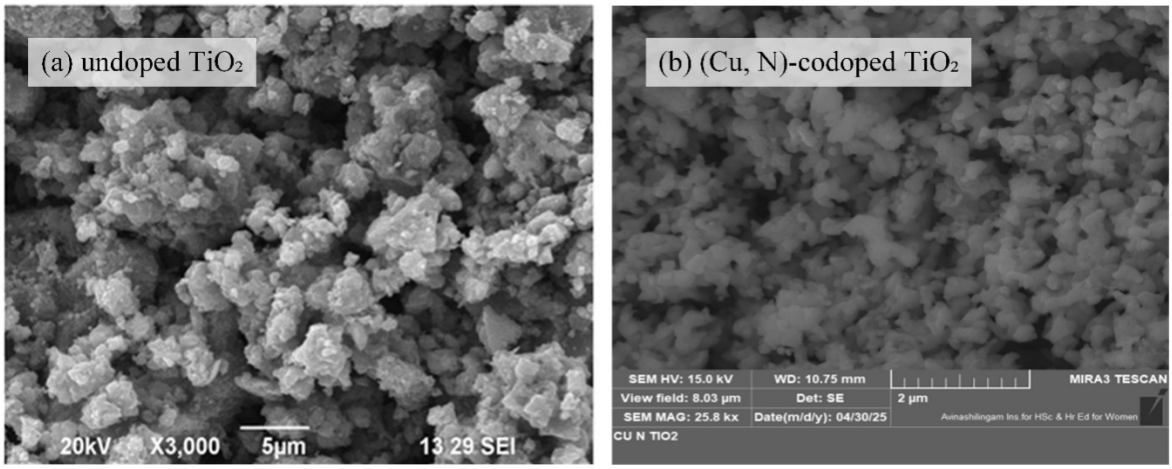

Fig. 5. SEM images of (a) undoped TiO_2 and (b)(Cu,N)-codopedTiO_2 photocatalysts

Energy Dispersive X-ray (EDX) spectroscopy analysis

Energy Dispersive X-ray (EDX) spectroscopy was performed to verify the chemical composition of the undoped TiO_2 and (Cu, N)-codopedTiO_2 photocatalysts, as shown in Fig. 6(a) and Fig. 6(b) respectively. The EDX spectra confirm the successful synthesis of undoped TiO_2 and (Cu, N)-codopedTiO_2 photocatalysts, with additional Cu and N peaks indicating successful co-doping. Quantitative analysis (Ti: 80.79 wt%, O: 13.29 wt%, Cu: 5.43 wt%, N: 0.49 wt %) demonstrates controlled doping without secondary phases. The absence of additional impurity peaks further confirms the high purity of the undoped TiO_2 and (Cu, N)-codopedTiO_2 photocatalysts [32, 33]. The substitution of Cu^{2+} for Ti^{4+} and N^{3-} into O^{2-} sites induces lattice distortion and band gap narrowing, enhancing visible-light photocatalytic activity [44].

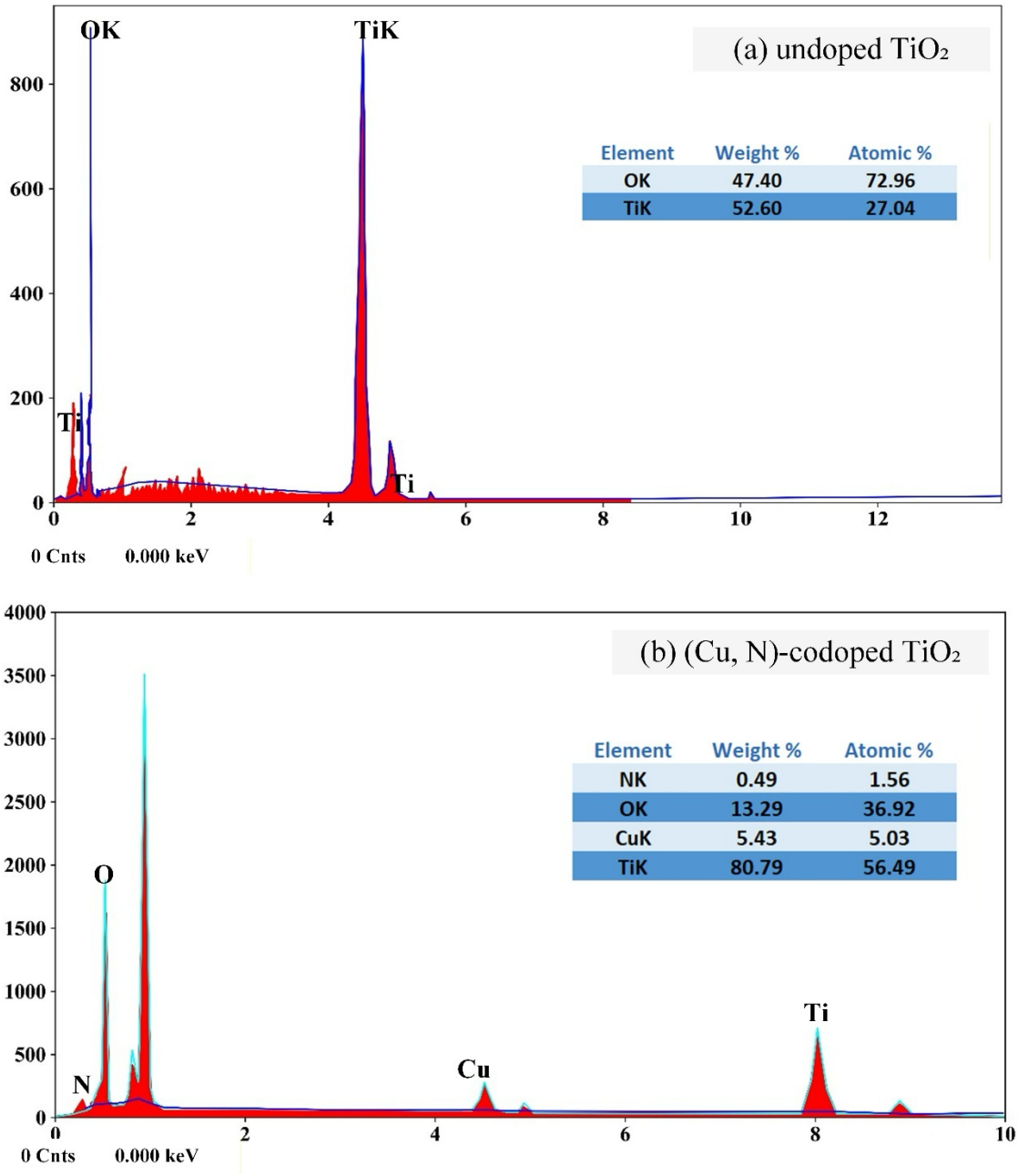

Fig.6. EDX pattern of (a) undoped TiO_2 and (b) (Cu, N)-codoped TiO_2 photocatalysts.

TEM Analysis

To investigate and characterize the morphology of undoped TiO_2 and (Cu, N)-codopedTiO_2 photocatalysts, TEM images are presented in Fig. 7(a) and Fig. 7(b). The observed lattice fringes correspond to the crystalline planes of TiO_2, confirming the well-defined crystalline nature of the materials. The TEM images of undopedTiO_2 and (Cu, N)-codopedTiO_2 photocatalysts reveal that the nanoparticles exhibit a predominantly spherical morphology with slight aggregation. The particle sizes are distributed in the range of 10–30 nm.

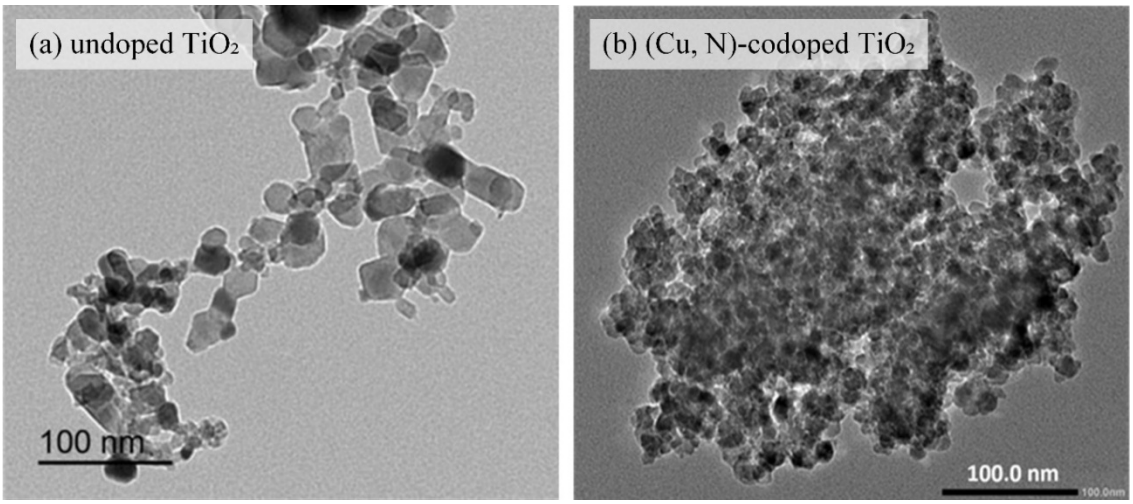

Fig.7. HR-TEM images of (a) undoped $TiO_2$and (b) (Cu,N)-codopedTiO_2photocatalysts

The particle size distribution histograms, obtained using Gaussian fitting, are shown in Fig. 8(a) and Fig. 8(b) respectively.From these images theaverage particle sizefor undoped TiO_2 and(Cu, N)codopedTiO_2 were calculated to be approximately 22 nm and 11.2 nm respectively. These findings are in good agreement with the results calculated from XRD pattern. The size of the photocatalysts in nanoscales crucial for enhancing their electronic, optical, and catalytic properties, leading to improved photocatalytic performance.

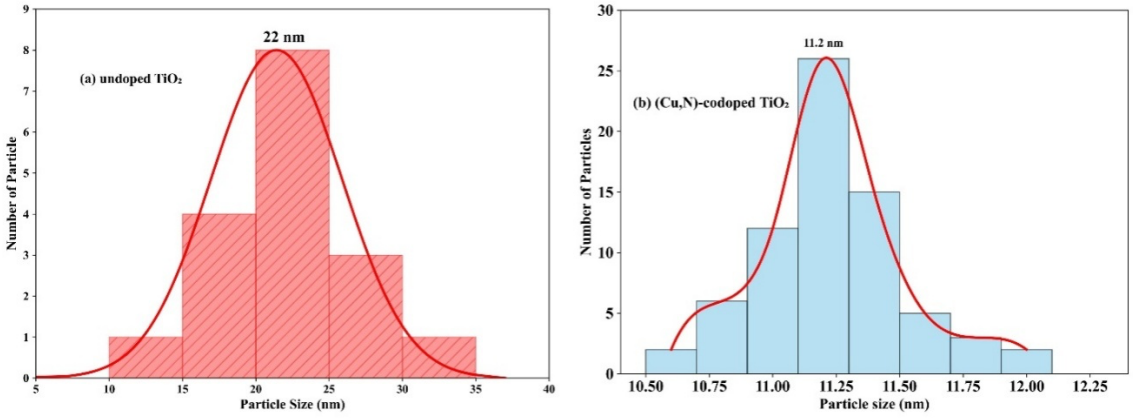

Fig.8. Particle size distribution of (a) undoped TiO_2 and (b) (Cu,N)-codoped TiO_2 photocatalysts

Diffuse Reflectance Spectroscopic(DRS) Analysis

The optical properties of undoped TiO_2 photocatalysts and (Cu, N)-codopedTiO_2 photocatalysts were investigated using a UV-Vis spectrometer in the wavelength range of 200–800 nm, as shown in Fig. 9(a) and Fig. 9(b), respectively. TheTauc relation, Equation (3) was used to calculate the optical energy band gap [47].

$$(\alpha h\nu) = A\left(h\nu - E_g\right)^n \quad (3)$$

Where,α is the absorption coefficient, $h\nu$ is the photon energy, A is a constant, E_g is the optical band gap, and $n$denotes the transition type. The band gap was calculated by plotting $(\alpha h\nu)^2$ versus $h\nu$,

and the linear portion of the absorption edge was extrapolated to the energy axis to determine the band gap value.

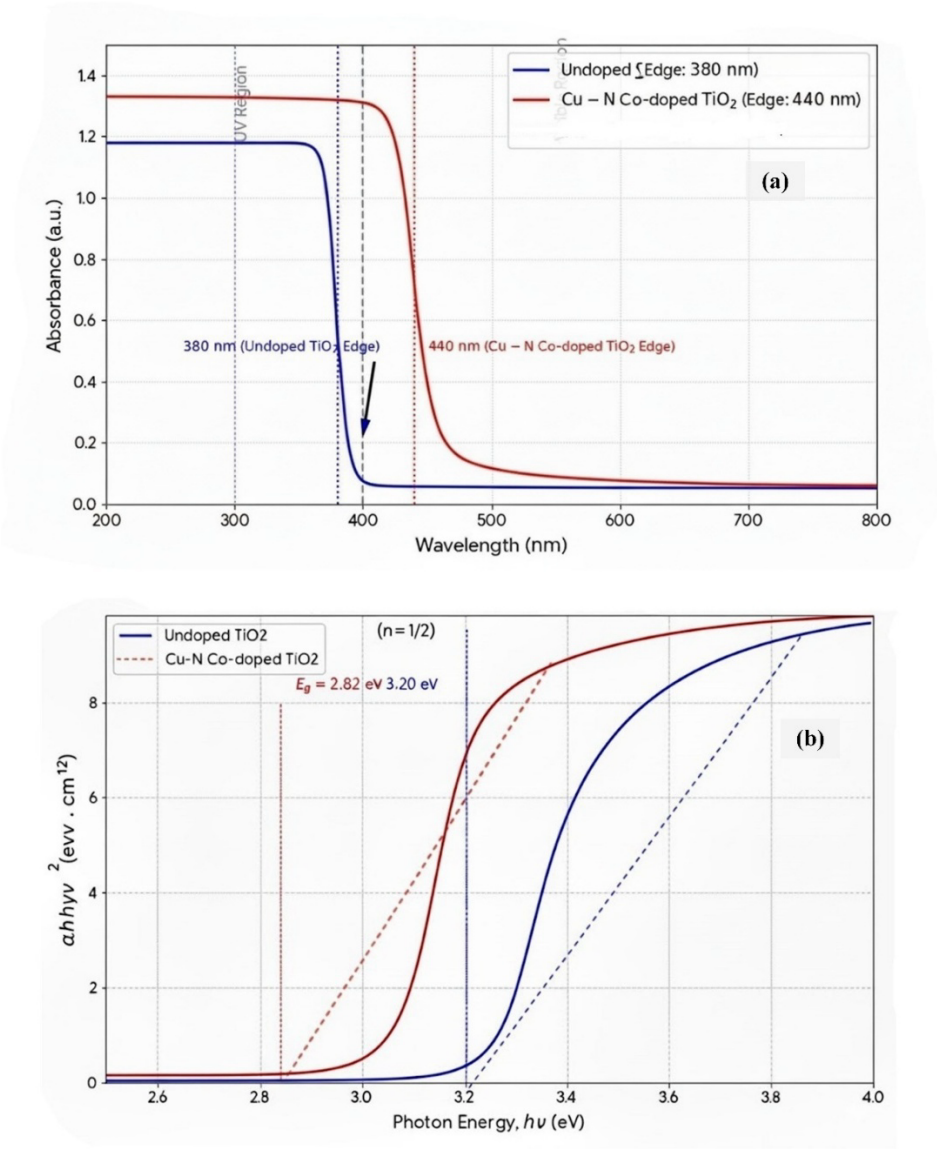

Fig.9. (a) UV-Visible absorption spectra and (b) Tauc plot for undoped $TiO_2$and (Cu, N)-codoped TiO_2 photocatalysts

The UV–visible absorption spectrum of undoped TiO_2 typically shows an absorption edge near 380 nm, corresponding to a band gap of about 3.2 eV [48], which limits its optical activity to the UV region. In contrast, the (Cu, N)-codopedTiO_2 sample exhibits a distinct redshift of the absorption edge toward the visible region (up to ~440 nm), indicating a reduction in the optical band gap to approximately 2.82 eV [49].This redshift is attributed to the introduction of localized energy levels within the band structure due to the hybridization ofCu 3d and N 2porbitals with TiO_2. The incorporation of these dopants effectively narrows the band gap, enabling visible-light absorption and improving

photocatalytic efficiency under solar irradiation. Thus, the observed spectral behavior confirms the successful codoping of Cu and N into the TiO_2 lattice and its enhanced optical response in the visible region [50].

The incorporation of Cu^{2+} and N^{3-} ions into the TiO_2 crystal lattice results in a narrowing of the band gap, enabling enhanced visible-light photocatalytic activity. Cu^{2+} ions introduce localized energy levels within the band gap, whereas N^{3-} ions form mid-gap states, collectively improving light absorption and facilitating efficient charge separation. This codoping strategy extends the photocatalytic response of TiO_2 into the visible spectrum, thereby enhancing the degradation efficiency of organic pollutants under visible-light irradiation [51, 52].

Photocatalytic investigation

The degradation of MY dye under solar lightirradiation was investigated using the synthesized undoped TiO_2 and (Cu, N)-codopedTiO_2 photocatalysts. The UV-Vis absorption spectra for the degradation of MY dye in the presence of (Cu, N)-codopedTiO_2 is displayed in Fig.10(a). The degradation process was assessed by monitoring the characteristicabsorption peak of MYdye at 425nm, which progressively diminished over time and disappeared completely after 40 minutes ofexposure.

To evaluate photolysis, the MYdye solution was exposed to sunlight for 40 minutes in the absence of a photocatalyst, as shown in Fig. 10(b). The results indicate that the dye exhibits minimal photolytic degradation. An additional experiment was conducted in the dark to assess dye removal due to adsorption on the photocatalyst surface. The degradation efficiency of MYin the dark was 8% and 39% for undoped and (Cu, N)-codopedTiOphotocatalysts,respectively.

Photocatalytic degradation reactions under direct solar irradiation using 0.15 g of photocatalyst in 100 mL of dye solution showed that after 40 minutes, the degradation efficiencies for undoped and (Cu, N)-codopedTiO_2 were 28% and 100%, respectively. Compared to undoped TiO_2, (Cu, N)-codopedTiO_2photocatalyst exhibited a significant enhancement in dye degradation efficiency. This improvement is attributed to the incorporation of Cu and N ions into the TiO_2 lattice, which induces structural defects, reduces crystal size (as confirmed by XRD), and enhances photocatalytic activity[52].

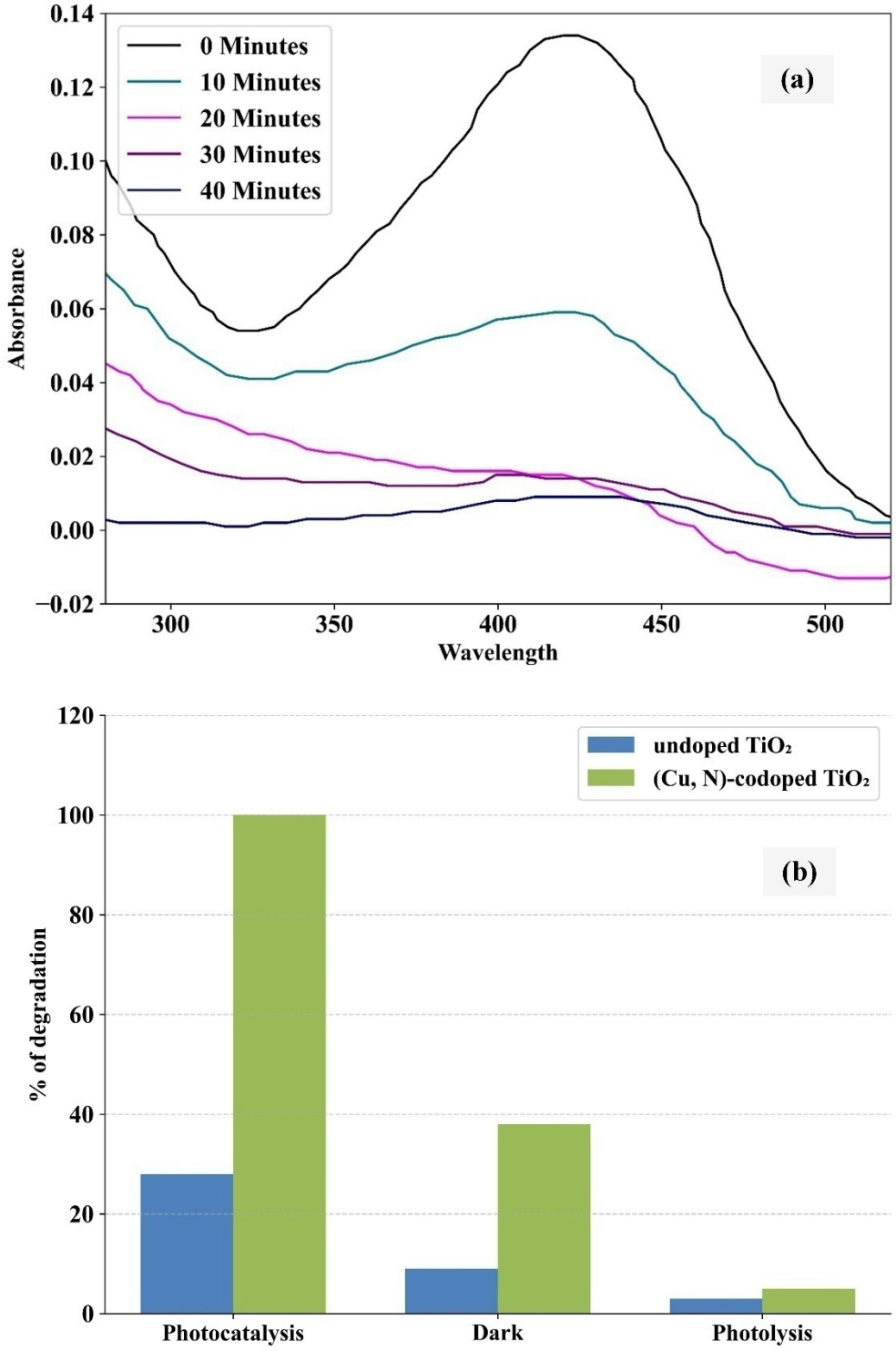

Fig.10. (a) Time dependent photocatalytic degradation of MY dye under solar light irradiation and (b) Comparative plot of degradation tendency of MY dye solution under different conditions.

UV–DRS analysis of (Cu, N)-codopedTiO_2photocatalyst showed a reduction in band gap energy, which enhances visible-light absorption and improves charge separation, resulting in superior photocatalytic performance. The effect of photocatalyst dosage revealed that increasing the amount of (Cu, N)-codopedTiO_2 increases the degradation efficiency of MY dye up to an optimal level, beyond which no significant improvement occurs due to light scattering and active site saturation. Under direct solar irradiation, (Cu, N)-codopedTiO_2 achieves almost complete dye degradation, than undoped TiO_2. These results confirm that (Cu, N)-codopedTiO_2 is an effective photocatalyst forthe complete mineralization ofMY dye from aqueous solution.

Effect of photocatalyst dosage

The effect of variation on amount of (Cu,N)-codopedTiO_2 photocatalyst on MY dye degradation was investigated at pH=7 for 40 minutes of solar light irradiation. The above investigation is done since insufficient use of photocatalyst leads to low rates of degradation due to a shortage of active sites. On the other hand, excessive use can result in light dispersion and clustering, which lowers efficiencyof dye degradation. Thus, the ideal amount strikes a balance between providing enough active sites and ensuring effective light absorption and interaction with the dye molecules [53].

The percentage of MY dye degradation (20ppm)was analyzed by varying the catalyst dosages, ranging from 0.5 to 0.2g/100 mL and is displayed in Fig.11. The percentagedegradation increased from 71% to 100% when the photocatalytic dosage was increased from 0.5 to 1.5g/100 mL. However, when the amount of catalyst was increased to 0.2g/100 mL, the degradation efficiency decreased to 79%. Thisreduction in degradation efficiency with increase in catalyst concentrations ascribeddue to the turbidity caused by excess catalyst in the test solution, which may block the penetration of visible light necessary to activate the reaction suspension [54]. Hence, the optimum dosage for the photocatalytic degradation of MY dye (20 ppm) by (Cu,N)-codopedTiO_2 was found to be 0.15 g/100 mL.

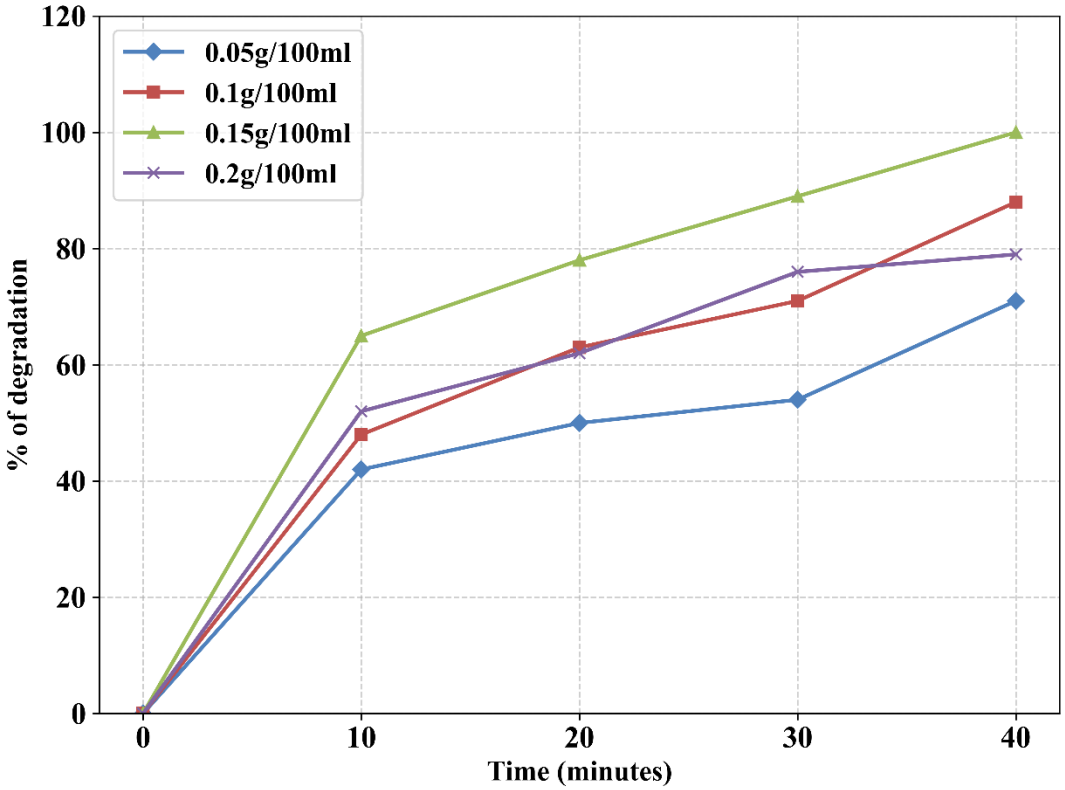

Fig.11. Effect of variation in the amount of (Cu, N)-codopedTiO₂photocatalyston % of degradation of MY dye

Effect of initial MY dye concentration

The effect of the initial dye concentration on the photocatalytic degradation process was studied by varying the initial concentration of dye solution with constant loading of (Cu, N)-codopedTiO₂photocatalyst(O.I5g/100mL)shown in Fig. 12. Degradation efficiency has increased from 86% to 100% as the concentration of dye was varied from 10 to 20 ppm. However, the percentage decreased from 100% to 89% as the concentration of dye solution was increased further above 20 ppm. The reason is, that the dye molecules competes for the active sites on the photocatalytic surface leading to overcrowding and thus decrease in degradation efficiency. Ahmad et al. observed that degradation efficiency initially increases with higher dye concentrations, likely because a greater number of dye molecules enhances the probability of interactions between the dye molecules and the photocatalyst, leading to a more efficient generation of reactive species, such as hydroxyl radicals. However, as the dye concentration continues to increase, the degradation efficiency decreases due to the saturation of active sites and the limited availability of reactive species. Thus, excessive dye concentrations hinder the photocatalytic process [55].

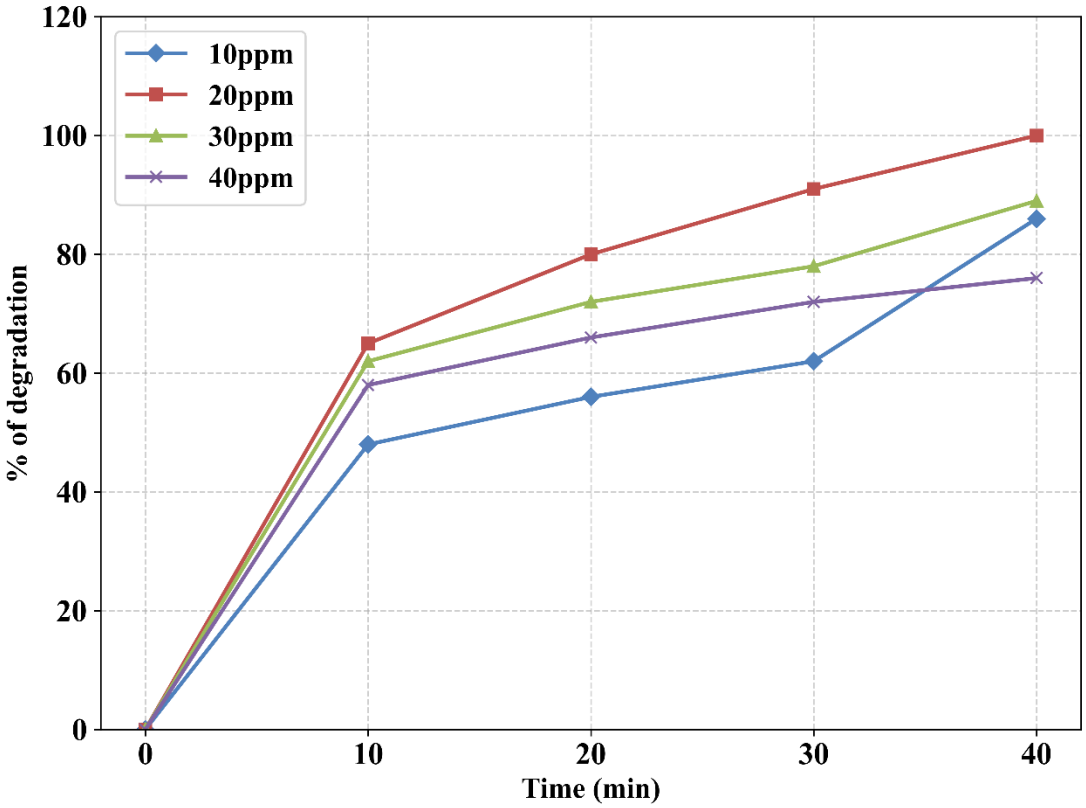

Fig. 12. Variation of initial dye concentration on the photocatalytic degradation of MY dye using 20ppm (Cu, N)-codopedTiO_2.

Effect of pH

The photocatalytic degradation of MY dye (20 ppm) using (Cu,N)-codopedTiO_2, 0.15g/100mL photocatalystis significantly influenced by pH. This study examined how changes in pH affected the rate of degradation when exposed to solar light. The pH range of 2–10 was used to examine the influence of pH on the MY dye degradation. At pH 6, the degradation efficiency dramatically increased, reaching 100% for 40 minutes of irradiation, as seen in Fig. 13.

When the pH was increased further from 6 to 10, nosignificant change in degradation efficiency was observed.At pH 10, the alkaline conditions showed the lowestdegradation efficiency (69%). According to these findings, dye degradation is considerably more effective in acidic media while being less effective in neutral and basic media. This enhancement is attributed to the formation of superoxide anions ($O_2^{\bullet -}$) and the subsequent generation of hydroxyl radicals (•OH), which are crucial for photocatalytic degradation of contaminants [56]. Based on the above studies, it can be concluded that 20 ppm, MY dye, can be completely degraded using 0.15g/100mL, (Cu,N)-codopedTiO_2,photocatalyst at an acidic pH 6 under 40 minutes of irradiation.

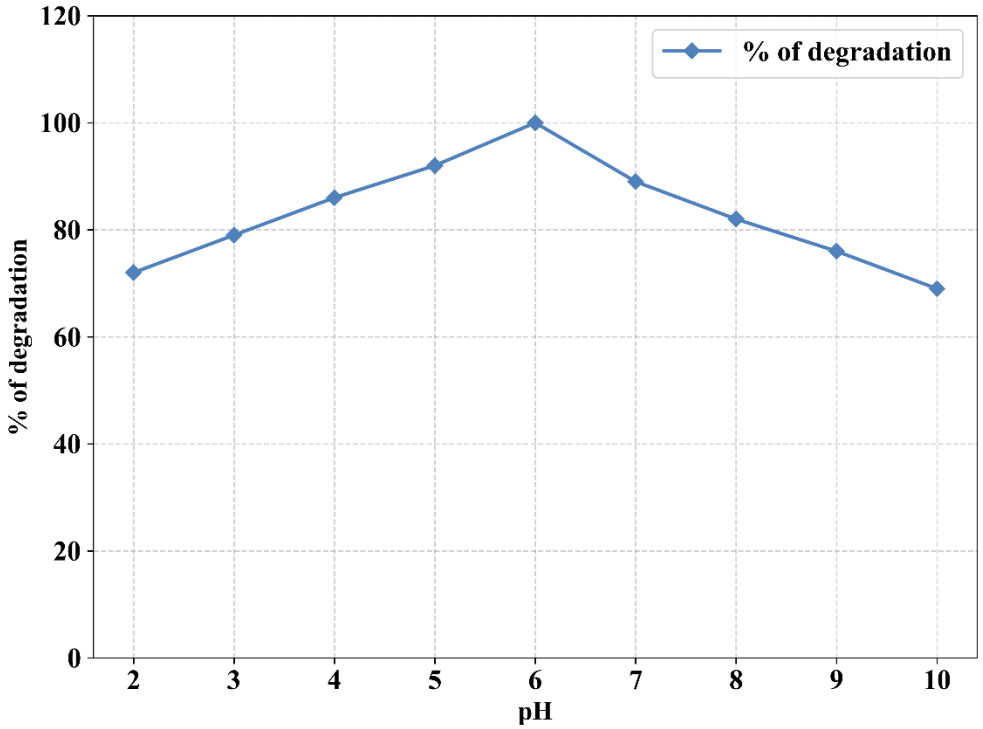

Fig. 13. Effect onvariation of pH on the photocatalytic degradation of MY dye using (Cu, N)-codopedTiO$_2$

Kinetics

The Langmuir–Hinshelwood kinetic model was used to describe the kinetics of photocatalytic reactions. The rate of the reaction is expressed in Equation (4).

$$r = \frac{dc}{dt} = K\frac{kc}{t} + kc \quad (4)$$

Where$r$, is the rate of the reaction, t is the time taken, k is the rate constant of the reaction, c is the concentration of the reactant and$K$ is the adsorption coefficient of the reactant. When the concentration c is small, the Equation (4)simplifies to a reliable first-order equation as given in Equation (5).

$$\ln\frac{c_0}{c_t} = kt \quad (5)$$

The linear plots shown in Fig. 14 indicate that the reaction followed pseudo-first-order kinetics [57-59]. The rate constant (k) for (Cu, N)-codopedTiO$_2$ photocatalysts toward the degradation of MYdye wascalculated as **0.051**×10^{-3} **min^{-1}** with a regression value of 0.978.

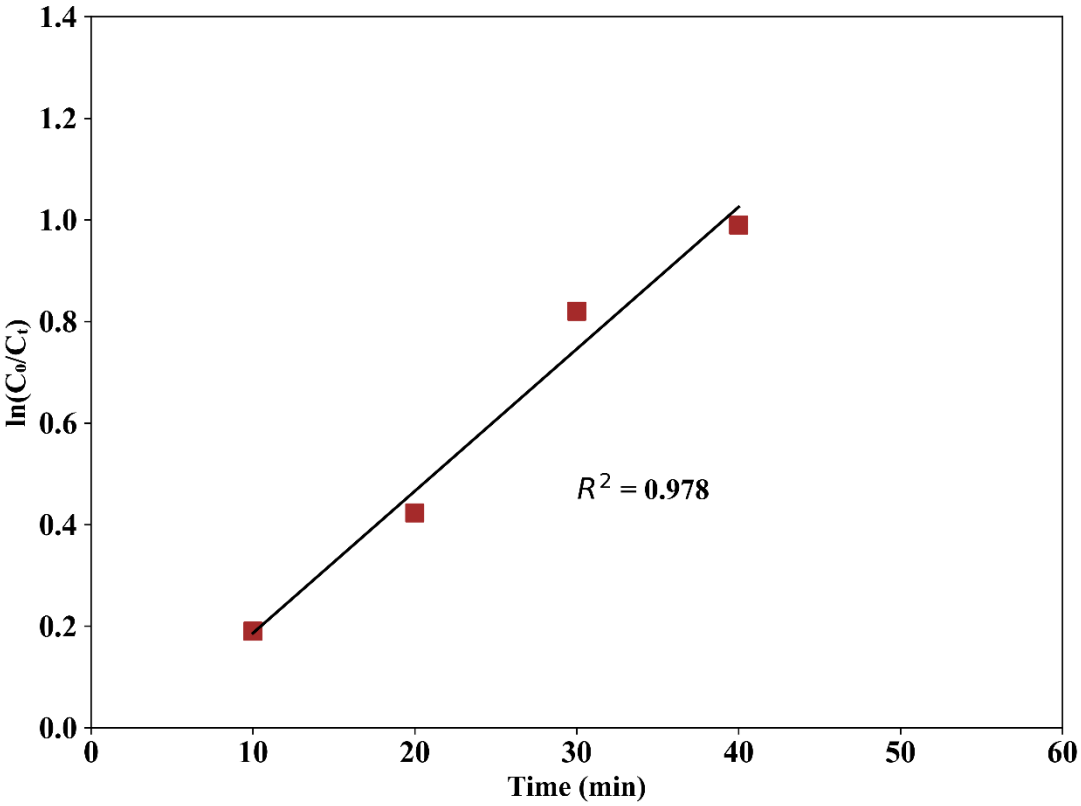

Fig .14. Kinetics of the photocatalytic degradation of MY dye 20ppm using 0.15g/100mL (Cu, N)-codopedTiO_2 photocatalyst

Photodegradation mechanism

The photomineralization process using (Cu, N)-codoped TiO_2 photocatalyst under sunlight irradiation generally involves photoexcitation, surface oxidation, reduction reactions, charge migration, which collectively contribute to the photooxidation of organic matter [60]. The photocatalyst is excited, resulting in the production of reactive species such as$O_2^{\bullet -}$,•OH and h^+. These reactive species are responsible for the degradation of MYdye when exposed to sunlight in the presence of the (Cu, N)-codopedTiO_2 photocatalyst.

$$(Cu,N)-TiO_2 + \text{sunlight} \longrightarrow (Cu,N)-TiO_2(e_{CB}^-) + (Cu,N)TiO_2(h_{VB}^+) \quad (6)$$

$$(Cu,N)-TiO_2(h_{VB}^+) + H_2O \longrightarrow (Cu,N)-TiO_2 + {}^{\bullet}OH + H^+ \quad (7)$$

$$(Cu,N)-TiO_2(e_{CB}^-) + O_2 \longrightarrow (Cu,N)-TiO_2 + O_2^{\bullet -} \quad (8)$$

$$(Cu,N)-TiO_2(e_{CB}^-) + O_2^{\bullet -} + 2H^+ \longrightarrow (Cu,N)-TiO_2 + H_2O_2^- \quad (9)$$

$$(Cu,N)-TiO_2(e_{CB}^-) + H_2O_2 \longrightarrow (Cu,N)-TiO_2 + {}^{\bullet}OH + OH^- \quad (10)$$

$${}^{\bullet}OH/O_2^{\bullet -} + \text{Metanil yellow} \longrightarrow \text{Intermediates} + \text{Degraded product}(CO_2 + H_2O + \cdots) \quad (11)$$

Oxygen molecules (O_2) can be reduced by the electrons generated on the doped photocatalyst to superoxide anion radicals ($O_2^{\bullet-}$), which play a crucial role in scavenging organic molecules and converting them into hydrogen peroxide or organic peroxides. Furthermore, the production of hydroxyl radical species ($^{\bullet}OH$), which drive the mineralization of MY, is largely caused by the conduction band electrons [61]. Fig. 15 sschematic representation of dye degradation mechanism for the (Cu, N)-codopedTiO₂ photocatalyst.

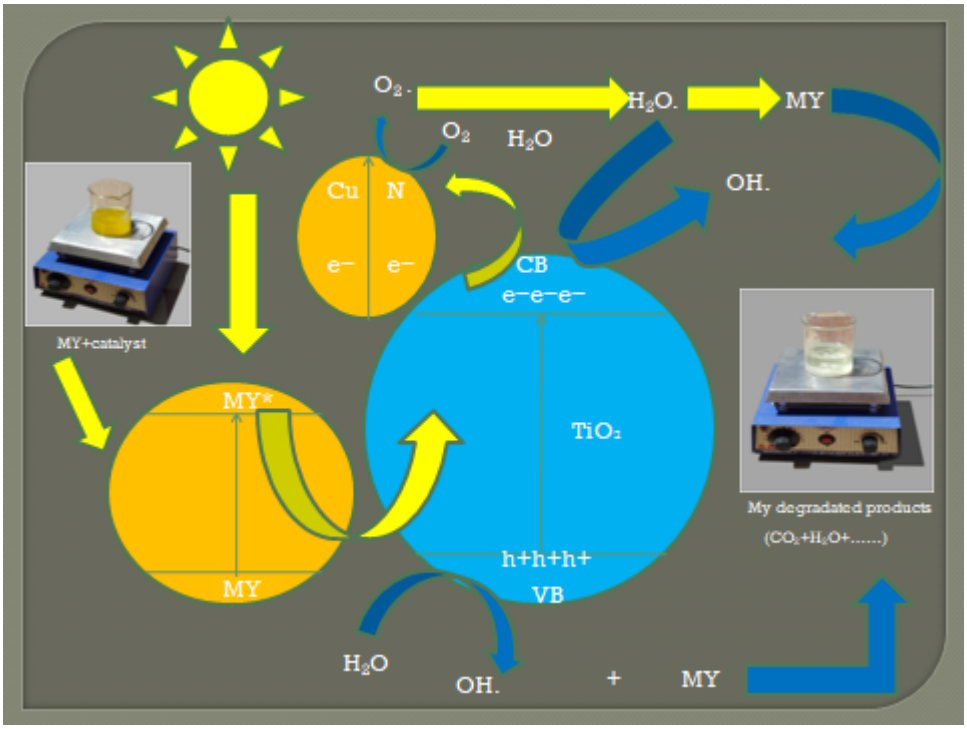

Fig: 15.Schematic diagram for the photocatalytic degradation mechanism of MY dye using(Cu, N)-codoped TiO_2.

Chemical Oxygen Demand (COD) Analysis

The synthesized (Cu, N)-codoped TiO_2 photocatalysthasshownexcellent potential for wastewater treatment by successfully reducing thechemical oxygen demand (COD) of My dye solution[62]. In this present study, COD of My dye solution was measuredbefore and after the photocatalytic degradation. Initially,the COD was approximately 14,458 mg/L. After treatment with (Cu,N)-codoped TiO_2photocatalyst under sunlight irradiation for 40 minutes, the COD was drastically reduced to 35mg/L, indicating nearly complete mineralization of the dye molecules and effective removal of color from the solution. These findings demonstrate the excellent degradation efficiency of organic contaminants by the synthesized (Cu, N)-codopedTiO₂ photocatalyst, indicating a possible solution for wastewater treatment.

Total Organic Carbon Analysis

To evaluate the mineralization of organic pollutants and their degradation products during the photocatalytic process, total organic carbon (TOC) analysis was analyzedbefore and after the

photocatalytic degradationofthe MY dye solution. The organic carbon content was significantly, indicating the effective breakdown of the organic componentsshowing 99.76 % removal efficiency. These results confirm that the synthesized(Cu, N)-codoped TiO_2photocatalystis highly effective in rapidly degrading the toxic organic pollutants in water.

Turnover frequency of the catalyst

Fig. 16 shows the photostability and recycling capacityof the synthesized (Cu, N)-codopedTiO_2photocatalyst.The photocatalyst was collected by centrifugation after each experiment run, rinsed several times, dried overnight, and reused for the consecutive cycles.The catalyst retained its activity for five cycles showing 100% removal efficiency and then showing 95 % in the sixth cycle, indicating good reusability and stability of the photocatalyst. These results confirm that the synthesized (Cu, N)-codoped TiO_2 photocatalystremoves organic pollutants from aqueous solutions. Finally, the results from this study were statistically compared with other reported photocatalysts as shown in Table 2.

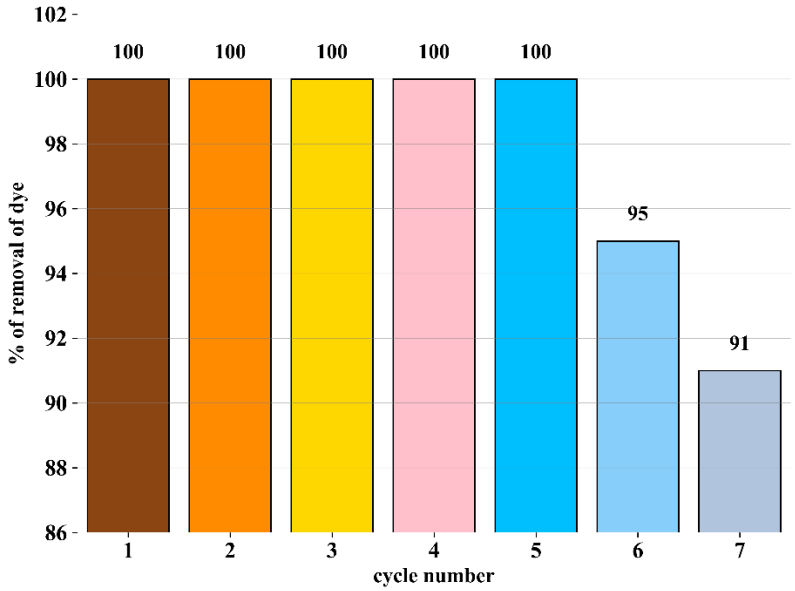

Fig.16.Recycling ability of synthesized (Cu, N)-cooped TiO_2photo catalyst.

Table2. Comparison of (Cu, N)-cooped TiO_2MY dye removal performance with other existing photocatalysts

Photocatalyst	Pollutant	Light Source	Time (min)	Degradation rate (%)	Reference
(Cu, N)-cooped TiO_2	Metanil Yellow	Visible light	40	100	This study
TiO_2-β-	Metanil	UV light	60	Enhanced	Sangari[63]

cyclodextrin (TiO_2/β-CD)	Yellow			decolouration efficiency compared to undoped TiO_2	
Polypyrrole based CuO-ZnO nanocomposite (PpCZ)	Metanil Yellow	Visible light	Not specified	~90	Biju et al. [64]
ZnO nanocrystals (green-synthesized)	Metanil Yellow	UV light	100	97	Priyadharshini et al. [65]

CONCLUSION

In the present study, undoped TiO_2 and (Cu,N)-codopedTiO_2 photocatalysts were successfully synthesized and characterized using various spectroscopic techniques. The XRD analysis confirmed that (Cu,N)-codopedTiO_2 has retained the intrinsic tetragonal anatase structure of TiO_2 without the formation of any secondary phases. Further, structural on the morphological studiesusing SEM analysis confirmed that, incorporation of Cu, N ions maintained a uniform distribution of particles with slight agglomeration, indicating a homogeneous dopant distribution on the TiO_2 surface.Energy dispersive X-ray(EDX) analysis confirmed the successful incorporation of Cu and N into the TiO_2 lattice without impurity phases, verifying controlled co-doping and high sample purity.TEM analysis revealed that both undoped and (Cu, N)-codopedTiO_2 nanoparticles exhibit predominantly spherical morphology withaggregation and well-defined crystallinity, supporting enhanced photocatalytic performance.UV–visible analysis revealed that the band gap of TiO_2has decreased from 3.2 eV to 2.82 eV with Cu, N codoping, enhancing visible-light absorption and photocatalytic activity.Undoped TiO_2 and (Cu, N)-codopedTiO_2 (0.15 mg/100 mL) photocatalysts removed 28% and 100% of Metanil Yellow (20 ppm) under sunlight within 40 minutes of sunlight irradiationrespectively, demonstrating superior dye degradationperformance for the codoped sample.Kinetic analysis using theLangmuir-Hinshelwood model indicated pseudo-first-order behavior. Completemineralization of MetanilYellow was further confirmed byreductions in COD and TOCmeasurements.The (Cu, N)-codopedTiO_2 nanophotocatalyst exhibited excellent stability and reusability over five successive cycles without loss of photocatalytic activity. These results confirm that Cu and N codoping is an effective strategy to enhance the visible-light photocatalytic performance of TiO_2 for environmental remediation.

ACKNOWLEDGEMENT

The authors are thankful to Karunya Institute of Technology and Science, Coimbatore, India; Abdul Kalam Research Centre, Sacred Heart College (Autonomous),Tirupattur District, India; and Alagappa University, Karaikudi, India, for providing the necessary resources and support for this work.

CONFLICT OF INTEREST

The authors declare no conflict of interest.

REFERENCES

[1] Tong, Y., Huang, Z., Janssen, A.B., Wishart, M., He, W., Wang, X. and Zhao, Y., 2022. Influence of social and environmental drivers on nutrient concentrations and ratios in lakes: A comparison between China and Europe. *Water Research*, *227*, p.119347.

[2]Almroth, B.C.,Cartine, J., Jönander, C., Karlsson, M., Langlois, J., Lindström, M., Lundin, J., Melander, N., Pesqueda, A., Rahmqvist, I. and Renaux, J., 2021. Assessing the effects of textile leachates in fish using multiple testing methods: From gene expression to behavior. *Ecotoxicology and Environmental Safety*, *207*, p.111523.

[3] Al-Tohamy, R., Ali, S.S., Li, F., Okasha, K.M., Mahmoud, Y.A.G., Elsamahy, T., Jiao, H., Fu, Y. and Sun, J., 2022. A critical review on the treatment of dye-containing wastewater: Ecotoxicological and health concerns of textile dyes and possible remediation approaches for environmental safety. *Ecotoxicology and environmental safety*, *231*, p.113160.

[4] Dutta, S. and Bhattacharjee, J., 2022. A comparative study between physicochemical and biological methods for effective removal of textile dye from wastewater. In *Development in wastewater treatment research and processes* (pp. 1-21). Elsevier.

[5]Jaafar, A., El-Husseini, S., Platas-Iglesias, C. and Bilbeisi, R.A., 2022. Zeolitic imidazolate framework (AMCD-ZIF) functionalised membrane for the removal of dyes from water. *Journal of Environmental Chemical Engineering*, *10*(3), p.108019.

[6] Al-Tohamy, R., Ali, S.S., Li, F., Okasha, K.M., Mahmoud, Y.A.G., Elsamahy, T., Jiao, H., Fu, Y. and Sun, J., 2022. A critical review on the treatment of dye-containing wastewater: Ecotoxicological and health concerns of textile dyes and possible remediation approaches for environmental safety. *Ecotoxicology and environmental safety*, *231*, p.113160.

[7] Elgarahy, A.M., Elwakeel, K.Z., Mohammad, S.H. and Elshoubaky, G.A., 2021. A critical review of biosorption of dyes, heavy metals and metalloids from wastewater as an efficient and green process. *Cleaner Engineering and Technology*, *4*, p.100209.

[8] Khader, E.H., Muslim, S.A., Saady, N.M.C., Ali, N.S., Salih, I.K., Mohammed, T.J., Albayati, T.M. and Zendehboudi, S., 2024. Recent advances in photocatalytic advanced oxidation processes for organic compound degradation: A review. *Desalination and Water Treatment*, *318*, p.100384.

[9] Geldasa, F.T., Kebede, M.A., Shura, M.W. and Hone, F.G., 2023. Experimental and computational study of metal oxide nanoparticles for the photocatalytic degradation of organic pollutants: a review. *RSC advances*, *13*(27), pp.18404-18442.

[10] Lupu, G.I., Orbeci, C., Bobirică, L., Bobirică, C. and Pascu, L.F., 2023. Key principles of advanced oxidation processes: A systematic analysis of current and future perspectives of the removal of antibiotics from wastewater. *Catalysts*, *13*(9), p.1280.

[11] Khan, Z.U.H., Gul, N.S., Sabahat, S., Sun, J., Tahir, K., Shah, N.S., Muhammad, N., Rahim, A., Imran, M., Iqbal, J. and Khan, T.M., 2023. Removal of organic pollutants through hydroxyl radical-based advanced oxidation processes. *Ecotoxicology and Environmental Safety*, *267*, p.115564.

[12] Tawfeek, S.E., Shalaby, A.M., Alabiad, M.A., Albackoosh, A.A.A.A., Albakoush, K.M.M. and

Omira, M.M.A., 2021. Metanil yellow promotes oxidative stress, astrogliosis, and apoptosis in the cerebellar cortex of adult male rat with possible protective effect of scutellarin: A histological and immunohistochemical study. *Tissue and Cell*, *73*, p.101624.
[13] Hausen, B.M., 1994. A case of allergic contact dermatitis due to metanil yellow. *Contact Dermatitis (01051873)*, *31*(2).
[14] EK, K.V., 2023. Solar light driven transition metal codopedZnO (Ag, Ni-codopedZnO) photocatalyst for environmental remediation. *Indian Journal of Chemical Technology (IJCT)*, *30*(3), pp.352-360.
[15]Uribe-López, M.C., Hidalgo-López, M.C., López-González, R., Frías-Márquez, D.M., Núñez-Nogueira, G., Hernández-Castillo, D. and Alvarez-Lemus, M.A., 2021. Photocatalytic activity of ZnO nanoparticles and the role of the synthesis method on their physical and chemical properties. *Journal of Photochemistry and photobiology A: Chemistry*, *404*, p.112866.
[16]Anucha, C.B., Altin, I., Bacaksiz, E. and Stathopoulos, V.N., 2022. Titanium dioxide (TiO_2)-based photocatalyst materials activity enhancement for contaminants of emerging concern (CECs) degradation: In the light of modification strategies. *Chemical Engineering Journal Advances*, *10*, p.100262.
[17]Sibhatu, A.K., Weldegebrieal, G.K., Sagadevan, S., Tran, N.N. and Hessel, V., 2022. Photocatalytic activity of CuO nanoparticles for organic and inorganic pollutants removal in wastewater remediation. *Chemosphere*, *300*, p.134623.
[18]Saini, S., Kaur, M., Pahwa, C. and Singh, S., 2024. Temperature Dependent Structural, Optical, Photocatalytic and Magnetic Properties of WO3 Nanoparticles. *Journal of Water and Environmental Nanotechnology*, *9*(3), pp.318-326.
[19]Jayaraj, S.K., Sadishkumar, V., Arun, T. and Thangadurai, P., 2018. Enhanced photocatalytic activity of V2O5 nanorods for the photodegradation of organic dyes: a detailed understanding of the mechanism and their antibacterial activity. *Materials Science in Semiconductor Processing*, *85*, pp.122-133.
[20]Basahel, S.N., Ali, T.T., Mokhtar, M. and Narasimharao, K., 2015. Influence of crystal structure of nanosized ZrO2 on photocatalytic degradation of methyl orange. *Nanoscale research letters*, *10*(1), p.73.
[21]Ezeibe Anderson, U., Nleonu Emmanuel, C., Onyemenonu Christopher, C. and Arrousse Nadia, N.C.C., 2022. Photocatalytic activity of aluminium oxide nanoparticles on degradation of ciprofloxacin. *Saudi J Eng Technol*, *7*(3), pp.132-136.
[22]Kim, S.P., Choi, M.Y. and Choi, H.C., 2016. Photocatalytic activity of SnO2 nanoparticles in methylene blue degradation. *Materials Research Bulletin*, *74*, pp.85-89.
[23]Duraisamy, N., Kandiah, K., Rajendran, R., S, P., R, R. and Dhanaraj, G., 2018. Electrochemical and photocatalytic investigation of nickel oxide for energy storage and wastewater treatment. *Research on Chemical Intermediates*, *44*(9), pp.5653-5667.

[24]Silva-Osuna, E.R., Vilchis-Nestor, A.R., Villarreal-Sanchez, R.C., Castro-Beltran, A. and Luque, P.A., 2022. Study of the optical properties of TiO2 semiconductor nanoparticles synthesized using Salvia rosmarinus and its effect on photocatalytic activity. *Optical Materials*, *124*, p.112039.
[25] Basavarajappa, P.S., Patil, S.B., Ganganagappa, N., Reddy, K.R., Raghu, A.V. and Reddy, C.V., 2020. Recent progress in metal-doped TiO2, non-metal doped/codoped TiO2 and TiO2 nanostructured hybrids for enhanced photocatalysis. *International journal of hydrogen energy*, *45*(13), pp.7764-7778.
[26]Fatima, R., Kadhem, A.A., Sajjad, A., Noman, H.M., Kiran, K.S., Kumar, S., Sunitha, S., Ray, S., Sariyevich, X.X., Fozil, X. and Shahid, M., 2025. Optimized Cu/Zr Co-doped TiO2 nanocomposites as high performance photocatalyst for visible light induced methylene blue degradation. *Journal of Alloys and Compounds*, p.184031.
[27] Yitagesu, G.B., Leku, D.T., Seyume, A.M., Workneh, G.A., 2024. Synthesis of TiO_2/CuO and its application for the photocatalytic removal of the methylene blue dye. *ACS Omega*, **9**(36), 39398126. https://doi.org/10.1021/acsomega.4c03472
[28] Sirivallop, A., Areerob, T. and Chiarakorn, S., 2020. Enhanced visible light photocatalytic activity of N and Ag doped and co-doped TiO2 synthesized by using an in-situ solvothermal method for gas phase ammonia removal. *Catalysts*, *10*(2), p.251.
[29]Faustino, E., da Silva, T.F., Cunha, R.F., Guelfi, D.R.V., Cavalheri, P.S., de Oliveira, S.C., Caires, A.R.L., Casagrande, G.A., Cavalcante, R.P. and Junior, A.M., 2022. Synthesis and characterization of N and Fe-doped TiO2 nanoparticles for 2, 4-Dimethylaniline mineralization. *Nanomaterials*, *12*(15), p.2538.
[30] Zhao, Z., Omer, A.A., Qin, Z., Osman, S., Xia, L. and Singh, R.P., 2020. Cu/N-codoped TiO2 prepared by the sol-gel method for phenanthrene removal under visible light irradiation. *Environmental Science and Pollution Research*, *27*(15), pp.17530-17540.
[31]Jaiswal, R., Bharambe, J., Patel, N., Dashora, A., Kothari, D.C. and Miotello, A., 2015. Copper and Nitrogen co-doped TiO2 photocatalyst with enhanced optical absorption and catalytic activity. *Applied Catalysis B: Environmental*, *168*, pp.333-341.
[32]Isari, A.A., Hayati, F., Kakavandi, B., Rostami, M., Motevassel, M. and Dehghanifard, E., 2020. N, Cu co-doped TiO2@ functionalized SWCNT photocatalyst coupled with ultrasound and visible-light: an effective sono-photocatalysis process for pharmaceutical wastewaters treatment. *Chemical Engineering Journal*, *392*, p.123685.
[33]Choi, J., Park, H. and Hoffmann, M.R., 2010. Effects of single metal-ion doping on the visible-light photoreactivity of TiO2. *The Journal of Physical Chemistry C*, *114*(2), pp.783-792.
[34]Shannon, R.D., 1976. Revised effective ionic radii and systematic studies of interatomic distances in halides and chalcogenides. *Foundations of Crystallography*, *32*(5), pp.751-767.
[35]Lin, Y.H., Hsueh, H.T., Chang, C.W. and Chu, H., 2016. The visible light-driven photodegradation of dimethyl sulfide on S-doped TiO2: Characterization, kinetics, and reaction pathways. *Applied Catalysis B: Environmental*, *199*, pp.1-10.

[36]Wu, M., Yang, B., Lv, Y., Fu, Z., Xu, J., Guo, T. and Zhao, Y., 2010. Efficient one-pot synthesis of Ag nanoparticles loaded on N-doped multiphase TiO2 hollow nanorod arrays with enhanced photocatalytic activity. *Applied Surface Science*, *256*(23), pp.7125-7130.
[37]Jeyachitra, R., Kalpana, S., Senthil, T.S. and Kang, M., 2020. Electrical behavior and enhanced photocatalytic activity of (Ag, Ni) co-doped ZnO nanoparticles synthesized from co-precipitation technique. Water Science and Technology, 81(6), pp.1296-1307.
[38] Thongpool, V., Phunpueok, A., Jaiyen, S. and Sornkwan, T., 2020. Synthesis and photocatalytic activity of copper and nitrogen co-doped titanium dioxide nanoparticles. *Results in Physics*, *16*, p.102948.
[39] Ahmadiasl, R., Moussavi, G., Shekoohiyan, S. and Razavian, F., 2022. Synthesis of Cu-doped TiO2 nanocatalyst for the enhanced photocatalytic degradation and mineralization of gabapentin under UVA/LED irradiation: characterization and photocatalytic activity. *Catalysts*, *12*(11), p.1310.
[40]Lian, P., Qin, A., Liu, Z., Ma, H., Liao, L., Zhang, K. and Li, N., 2024. Facile synthesis to porous TiO2 nanostructures at low temperature for efficient visible-light degradation of tetracycline. *Nanomaterials*, *14*(11), p.943.
[41]León, A., Reuquen, P., Garín, C., Segura, R., Vargas, P., Zapata, P. and Orihuela, P.A., 2017. FTIR and Raman characterization of TiO2 nanoparticles coated with polyethylene glycol as carrier for 2-methoxyestradiol. *Applied Sciences*, *7*(1), p.49.
[42]ROMÂNĂ, A., 2024. FT-IR SPECTROSCOPY STUDY OF THE TiO2 BASED POWDERS PREPARED BY THE SOL-GEL METHOD. *Rev. Roum. Chim*, *69*(10-12), pp.629-634.
[43] León, A., Reuquen, P., Garín, C., Segura, R., Vargas, P., Zapata, P. and Orihuela, P.A., 2017. FTIR and Raman characterization of TiO2 nanoparticles coated with polyethylene glycol as carrier for 2-methoxyestradiol. *Applied Sciences*, *7*(1), p.49.
[44]Janczarek, M. and Kowalska, E., 2017. On the origin of enhanced photocatalytic activity of copper-modified titania in the oxidative reaction systems. *Catalysts*, *7*(11), p.317.
[45]Raha, S. and Ahmaruzzaman, M., 2022. ZnO nanostructured materials and their potential applications: progress, challenges and perspectives. *Nanoscale advances*, *4*(8), pp.1868-1925.
[46] Liu, S., Yu, J. and Jaroniec, M., 2010. Tunable photocatalytic selectivity of hollow TiO2 microspheres composed of anatase polyhedra with exposed {001} facets. *Journal of the American Chemical Society*, *132*(34), pp.11914-11916.
[47] Fathi, S., Aslibeiki, B. and Torkamani, R., 2023. Oxytetracycline photodegradation by transition metals doped ZnO nanorods. *Journal of Water and Environmental Nanotechnology*, *8*(3), pp.254-266.
[48] Kumar, C. and Patra, S.N., 2022. Prediction of Bandgap of Undoped TiO2 for Dye-Sensitized Solar Cell Photoanode. *Applied Solar Energy*, *58*(4), pp.482-489.
[49] Mathur, A.S., Kumar, P. and Singh, B.P., 2018. Comparative study of absorption band edge tailoring by cationic and anionic doping in TiO2. *Mater Sci Poland*, *36*, pp.435-438.
[50]Goh, E.G., Xu, X. and McCormick, P.G., 2014. Effect of particle size on the UV absorbance of zinc oxide nanoparticles. *Scripta Materialia*, *78*, pp.49-52.

[51] Tian, F., Wu, Z., Yan, Y., Ye, B.C. and Liu, D., 2016. Synthesis of visible-light-responsive Cu and N-codoped AC/TiO2 photocatalyst through microwave irradiation. *Nanoscale Research Letters*, *11*(1), p.292.
[52] Suwondo, K.P., Alharissa, E.Z., Aprilita, N.H. and Tri Wahyuni, E., 2025. Remarkable Enhancement of TiO2–N Activity under Visible Light Exposure by Codoping with Cu from Electroplating Wastewater for Degradation of Amoxicillin Residual in Water Media. *ACS omega*, *10*(8), pp.7722-7733.
[53]Khan, S., Noor, T., Iqbal, N. and Yaqoob, L., 2024. Photocatalytic dye degradation from textile wastewater: a review. *ACS omega*, *9*(20), pp.21751-21767.
[54] Molla, M.A.I., Ahsan, S., Tateishi, I., Furukawa, M., Katsumata, H., Suzuki, T. and Kaneco, S., 2018. Degradation, kinetics, and mineralization in solar photocatalytic treatment of aqueous amitrole solution with titanium dioxide. *Environmental Engineering Science*, *35*(5), pp.401-407.
[55]Ahmad, I., Aslam, M., Jabeen, U., Zafar, M.N., Malghani, M.N.K., Alwadai, N., Alshammari, F.H., Almuslem, A.S. and Ullah, Z., 2022. ZnO and Ni-doped ZnO photocatalysts: Synthesis, characterization and improved visible light driven photocatalytic degradation of methylene blue. *InorganicaChimica Acta*, *543*, p.121167.
[56]Pawar, M.J., Nimbalkar, V.B., Khajone, A.D. and Deshmukh, S.B., 2021. Ag-Doped TiO 2 Synthesis, Characterization and Photodegradation of 4BS Dye. *Journal of Nanoscience and Technology*, pp.952-955.
[57] Stalin, S.S. and Kirupa Vasam Jino, E.K., 2023. Fabrication of Cu doped ZnO nanocrystals hybridised with Graphene oxide nanosheets as an efficient solar light driven photocatalyst for the degradation of Quinalphos pesticide in aqueous medium. *Journal of Water and Environmental Nanotechnology*, *8*(2), pp.94-107.
[58]Chen, X., Wu, Z., Liu, D. and Gao, Z., 2017. Preparation of ZnO photocatalyst for the efficient and rapid photocatalytic degradation of azo dyes. *Nanoscale research letters*, *12*(1), p.143.
[59]Singh, R., Barman, P.B. and Sharma, D., 2017. Synthesis, structural and optical properties of Ag doped ZnO nanoparticles with enhanced photocatalytic properties by photo degradation of organic dyes. *Journal of Materials Science: Materials in Electronics*, *28*(8), pp.5705-5717.
[60]Malwal, D. and Gopinath, P., 2016. Enhanced photocatalytic activity of hierarchical three dimensional metal oxide@ CuO nanostructures towards the degradation of Congo red dye under solar radiation. *Catalysis Science & Technology*, *6*(12), pp.4458-4472.
[61]Sin, J.C., Lam, S.M., Satoshi, I., Lee, K.T. and Mohamed, A.R., 2014. Sunlight photocatalytic activity enhancement and mechanism of novel europium-doped ZnO hierarchical micro/nanospheres for degradation of phenol. *Applied Catalysis B: Environmental*, *148*, pp.258-268.
[62]MohamadHanapi, N.H., Sayid Abdullah, S.H.Y., Khairuddin, Z., Mahmod, N.H., Monajemi, H., Ismail, A., Lananan, F., Suhaili, Z., Endut, A. and Juahir, H., 2022. COD removal and colour degradation of textile dye effluents by locally isolated microbes. *International Journal of Environmental Analytical Chemistry*, *102*(19), pp.7835-7850.

[63] Sangari, N.U., 2018. Role of β-cyclodextrin in enhanced photocatalytic decolorization of metanil yellow dye with TiO2. *Asian Journal of Chemistry*, *30*(10), pp.2294-2298.
[64] Biju, R., Ravikumar, R., Thomas, C. and Indulal, C.R., 2022. Enhanced photocatalytic degradation of Metanil Yellow dye using polypyrrole-based copper oxide–zinc oxide nanocomposites under visible light. *Journal of Nanoparticle Research*, *24*(6), p.117.
[65] Priyadharshini, S.S., Shubha, J.P., Shivalingappa, J., Adil, S.F., Kuniyil, M., Hatshan, M.R., Shaik, B. and Kavalli, K., 2021. Photocatalytic degradation of methylene blue and metanil yellow dyes using green synthesized zinc oxide (ZnO) nanocrystals. *Crystals*, *12*(1), p.22.